CdS nanofilms: effect of deposition temperature on morphology and optical band gap

2013 Phys. Scr. 88 045603

(http://iopscience.iop.org/1402-4896/88/4/045603)

Phys. Scr. **88** (2013) 045603 (8pp) doi:10.1088/0031-8949/88/04/045603

CdS nanofilms: effect of deposition temperature on morphology and optical band gap

Suresh Kumar, Pankaj Sharma and Vineet Sharma

Department of Physics and Materials Science, Jaypee University of Information Technology, Waknaghat, Solan, HP 173234, India

E-mail: pks_phy@yahoo.co.in (Pankaj Sharma)

Received 14 January 2013
Accepted for publication 6 September 2013
Published 26 September 2013
Online at stacks.iop.org/PhysScr/88/045603

Abstract

We have grown 45–60 nm thick uniform smooth cadmium sulphide (CdS) nanofilms via a chemical bath deposition technique at different deposition temperatures ($T_d = 50$, 60, 70, 80 and 90 °C) and these have been studied using x-ray diffraction, scanning electron microscopy, atomic force microscopy and a UV–Vis–NIR spectrophotometer. The growth rate increases with increasing T_d up to 70 °C and then decreases. The structural analysis shows that CdS nanofilms exist in cubic or polymorph phases. The surface analysis indicates that the morphology of the films changes with increasing T_d. CdS nanofilms grown at $T_d = 70$ °C show high transmittance, low absorbance with a higher band gap.

PACS numbers: 68.55.J−, 68.37.Ps, 78.67.−n, 88.40.jm

(Some figures may appear in color only in the online journal)

1. Introduction

Cadmium sulphide (CdS) films have been extensively studied in recent years for their scientific and technological applications in electronics, optoelectronics, photovoltaic, solar cells and nonlinear optics [1–5]. Bulk CdS is an n-type semiconductor with a direct band gap of 2.42 eV [4] and is a promising material for visible and near infrared range applications; particularly for solar cells and photodetectors [4–10]. For a photovoltaic solar cell, CdS films should have high transparency, suitable optical absorption, high photoconductivity and low film thickness to avoid absorption in the window layer. The film should be non-conductive to high short circuit current density [8, 11]. In the recent reports [5, 8, 12–14], there is scope to increase the cell efficiency up to 20% by reducing the thickness of the CdS window layer (<100 nm). In a solar cell, reduced CdS film thickness has been able to improve the blue spectral response [15, 16] and freely transmit the bulk of the solar spectrum. Thus, this makes it suitable as a window layer above the absorber in which photo generation of an excess minority carrier has taken place [17].

In practice, reduced film thickness may produce non-uniformity and discontinuities in the film microstructure resulting in a decrease of open circuit voltage and poor cell performance. The properties of chemical bath (CBD) deposited films may be controlled by various parameters like the concentration of reagents, deposition temperature, pH, complexing agent, etc [1, 11, 14, 18–21]. Deposition temperature significantly influences structural growth, deposition rate and reaction kinetics. Hence, the role of deposition temperature is extremely critical in CBD for the film growth and controlling different properties of the films [11, 22–25].

In the present work, we have deposited nanofilms (<100 nm) of CdS at different deposition temperatures. The structural, morphological and optical properties have been investigated for CdS nanofilms deposited at different temperatures i.e. $T_d = 50$C, 60, 70, 80 and 90 °C. The effect of T_d on the growth process and crystallite size has been investigated. The optical behaviour of deposited nanofilms with T_d has been analysed from transmittance (T%) and reflectance (R%) measurements.

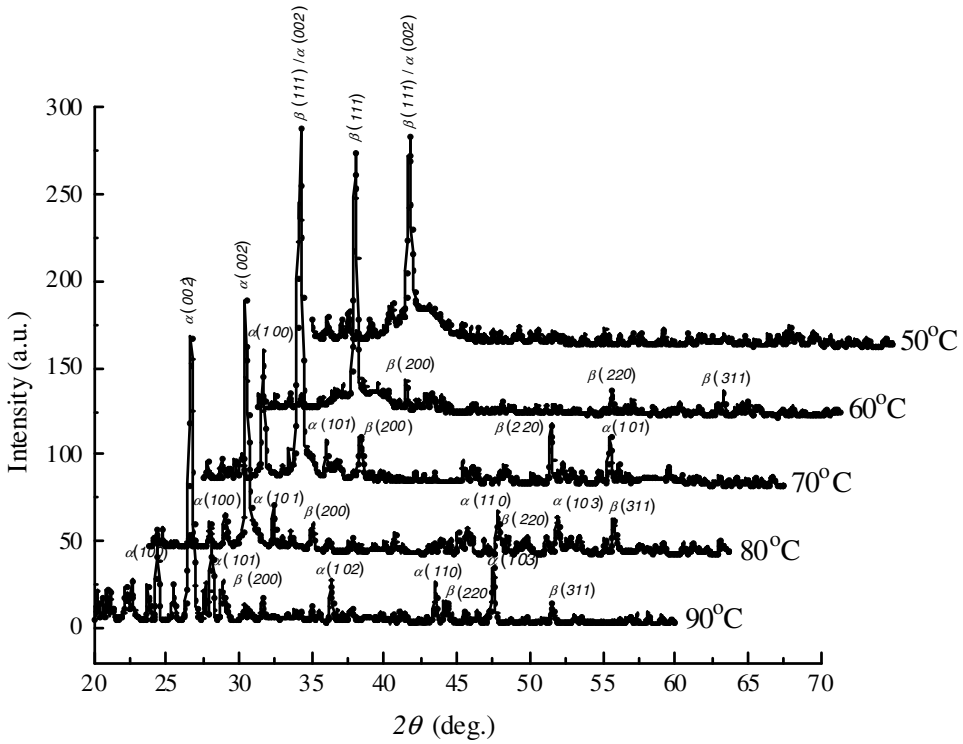

Figure 1. XRD spectra for as-deposited CdS nanofilms at different $T_d = 50$, 60, 70, 80 and 90 °C.

Table 1. Values of various structural parameters obtained for CdS nanofilms.

			WH method		DS method	AFM	
T_d(°C)	d_{hkl}(Å)	$D_{2\theta}$(nm)	D_v(nm)	$\varepsilon_{hkl} \times 10^{-3}$	$\delta_{hkl} \times 10^{15}$(line m^{-2})	Crystallite size (nm)	rms roughness (nm)
50	3.326	34.51	25.40	0.67	1.55	39	15.56
60	3.326	30.04	22.81	1.78	1.92	32	6.87
70	3.334	21.93	20.63	1.89	2.35	21	5.65
80	3.339	26.93	28.90	0.85	1.20	33	11.73
90	3.339	37.64	35.61	0.48	0.79	38	16.84

2. Experimental details

Chemicals used in the synthesis were of analytical grade (Merck, India) and used as received. The deposition of CdS nanofilms was done by the sequential addition of aqueous solution of cadmium chloride [$CdCl_2H_2O$:0.02 M], ammonia solution [NH_4OH :1 M] and double distilled water containing an appropriate amount of Triton (TX-100). A well cleaned and dried glass substrate was inserted vertically into the bath and the solution was heated up to the temperature of investigation i.e. (50–90 °C). Finally, at the deposition temperature (i.e. $T_d = 50$, 60, 70, 80 and 90 °C) the aqueous solution of thiourea [$(CSNH_2)_2$: 0.04 M] was added. The pH of the final solution was stabilized at 11 ± 0.1. The depositions were carried out for a period of 40 min. After the deposition, films were cleaned with double distilled water. The films have been thermally annealed in vacuum at 573 ± 5 K for 2 h. The obtained films were pale yellow to orange yellow in color, uniform and with a good adherence to the substrate.

The thickness of the deposited CdS nanofilms was measured using a stylus profilometer (AMBIOS XP-1). Elemental composition has been checked using an energy dispersive x-ray analyser (EDAX, Bruker equipped with analytical Software QUANTAX 200). The structural properties were analysed by x-ray diffraction (XRD, PANalytical's X'Pert-PRO) in the grazing angle mode. The surface morphology was studied by scanning electron microscopy (SEM, ZEISS EVO40) operated at 20 kV with 102 pA. The surface topography was studied using atomic force microscopy (AFM, NTMDT-NTEGRA) in semi-contact mode. *T*% and *R*% spectra were obtained by a UV–Vis–NIR double beam spectrophotometer (Perkin Elmer: Lambda-750) in the wavelength range 300–900 nm.

3. Results

XRD spectra (figure 1) shows that film deposited at 50 °C corresponds to a cubic-zinc blende (β-CdS) or hexagonal-wurtzite (α-CdS) structure[1]. With an increase in deposition temperature ($T_d \leqslant 70$ °C) easily identified phases appeared (β/α-CdS and β-CdS) and these phases are labelled in figure 1. Films deposited ($T_d > 70$ °C) have a prominent α-CdS phase. The interplanar spacing (d_{hkl}) values (table 1) calculated using Bragg's equation [26] are within a 1% error approximation (see footnote 1). The crystallite size ($D_{2\theta}$) for different deposition temperatures has been determined

[1] JCPDS X-ray Powder File Data (Data file 06-0314 and 89-0440).

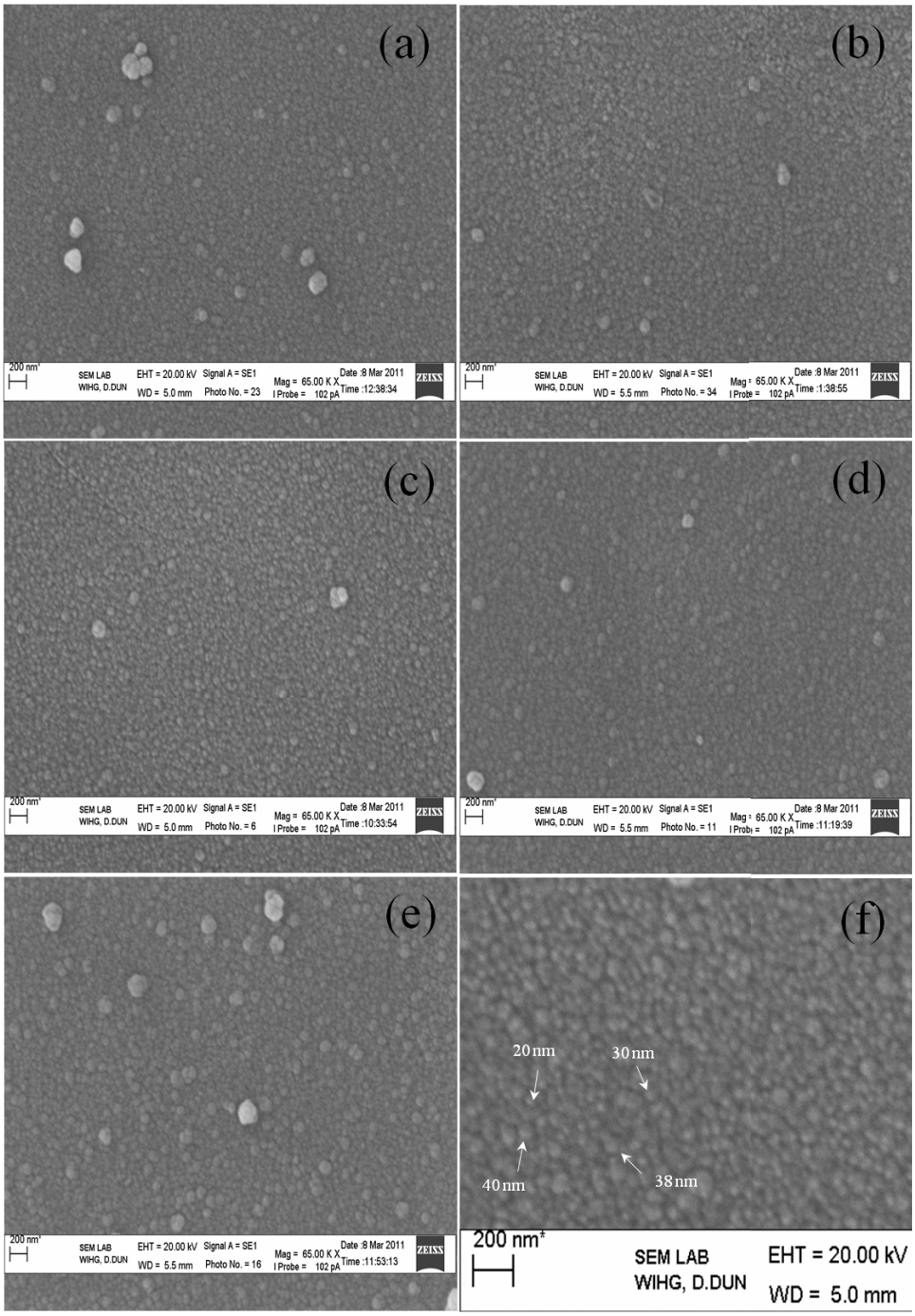

Figure 2. SEM images of CdS nanofilms deposited at (a) 50 °C, (b) 60 °C, (c) 70 °C, (d) 80 °C, (e) 90 °C and (f) zoomed image (70 °C) with estimated crystallite size.

(table 1) using the Debye–Scherrer (DS) method [27]. The significant broad profile of XRD peaks (figure 1) may be due to the presence of nanocrystallites, lattice defects and strain in the films. The crystallite size (D_v) and microstrain (ε_{hkl}) have been calculated (table 1) using the Williamson Hall (WH) method [28]. The dislocation density (δ_{hkl}) [29] has been calculated using the formula, $\delta_{hkl} = 1/D_v^2$ (table 1).

SEM micrographs of CdS nanofilms (figure 2) show that the surface of the films are smooth, homogeneous and free of pores and cracks. This may be due to the influence of the reducing agent TX-100 which eliminates gas bubble formation in the bath [29, 30]. SEM images with high magnification have been used to estimate the size of crystallites. The average crystallite size has been found to vary from 20 to 100 nm for films deposited at $T_d \neq 70$ °C, whereas at 70 °C average crystallite size varies from 20 to 40 nm (figure 2(f)).

AFM is an appropriate tool for topographical analysis of the film surfaces that provide information about crystallite size, surface texture and roughness. The surface topography of CdS nanofilms for a scan size of $1 \times 1\ \mu m^2$ are shown in figure 3. Topographic images for films deposited at $T_d \neq 70$ °C show compact and rough surfaces with large grain size. Films at $T_d = 70$ °C confirm a less compact but smooth surface with uniform nanocrystallites. The crystallite size and root mean

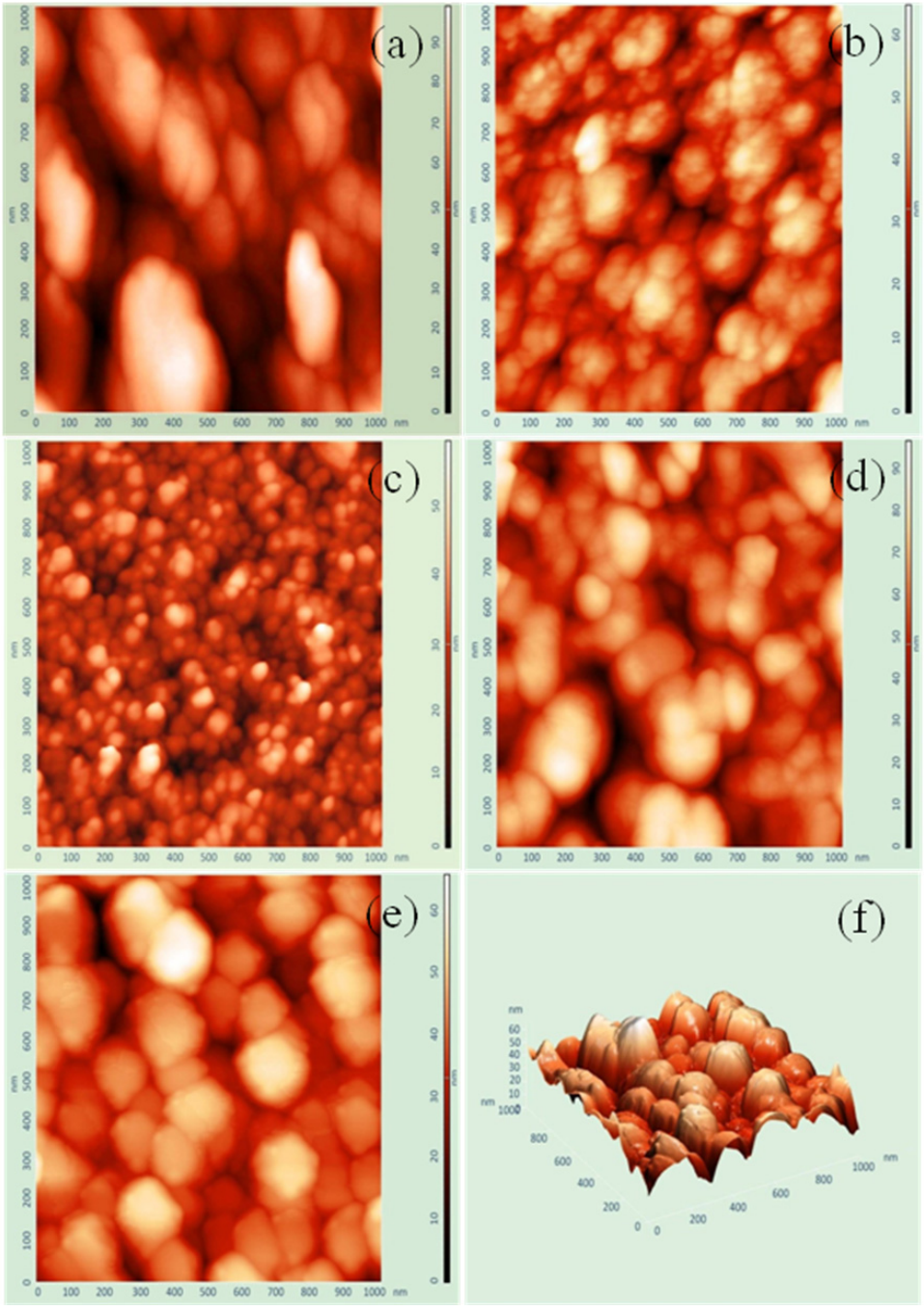

Figure 3. Two-dimensional AFM surface images of CdS nanofilms deposited at (a) 50 °C, (b) 60 °C, (c) 70 °C, (d) 80 °C, (e) 90 °C and (f) three-dimensional AFM image of nanofilms deposited at 90 °C.

square (rms) roughness (table 1) decrease to minimum for $T_d = 70\,^{\circ}\mathrm{C}$.

Figure 4 shows $T\%$ and $R\%$ spectra of CdS nanofilms at different T_d. $T\%$ in the low wavelength region extends up to 300 nm indicating the presence of disorders and amorphous components in the films [24]. The absorption coefficient (α) signifies inter-band transition near the band gap and has been calculated at the fundamental absorption edge [31]. Sharp increases in α near the fundamental absorption edge indicate a direct energy transition in the forbidden gap. The optical band gap (E_g) has been determined using Tauc's relation [32]. E_g values (table 2) have been estimated (figure 5) by extrapolation of $(\alpha h\nu)^2 \to 0$. It has been found that E_g increases to a maximum for $T_d = 70\,^{\circ}\mathrm{C}$.

The refractive index (n) and extinction coefficient (k) for CdS nanofilms have been calculated [19]. The refractive index value is maximal and the extinction coefficient is minimal for CdS nanofilms $T_d = 70\,^{\circ}\mathrm{C}$ (figure 6). The real ($\varepsilon_r = n^2 - k^2$) and imaginary part ($\varepsilon_i = 2nk$) of the dielectric constant have been calculated in the visible region [32] and at $T_d = 70\,^{\circ}\mathrm{C}$, ε_r is maximum and ε_i is minimum (figure 7).

4. Discussion

The noise and diffused background in figure 1 may be due to the presence of some amorphous component and low film thickness of CdS nanofilms. The films deposited at $T_d < 70\,^{\circ}\mathrm{C}$ have a predominantly cubic structure, whereas

Table 2. Values of optical parameters for CdS nanofilms at various deposition temperatures.

T_d (°C)	$\alpha \times 10^4 (cm^{-1})$	E_g (eV)	E_g^{sub} (eV)	$B \times 10^9$ (cm^{-2} eV^{-1})	E_u (eV)	$\sigma \times 10^{14} (\Omega^{-1} m^{-1})$
50	5.08	2.43 ± 0.01	2.15 ± 0.01	4.89	0.537	2.97
60	4.49	2.51 ± 0.01	2.20 ± 0.01	3.51	0.520	2.60
70	3.59	2.88 ± 0.01	2.30 ± 0.01	1.71	0.471	2.43
80	4.36	2.68 ± 0.01	2.27 ± 0.01	2.83	0.534	2.49
90	4.83	2.52 ± 0.01	2.20 ± 0.01	3.03	0.544	2.59

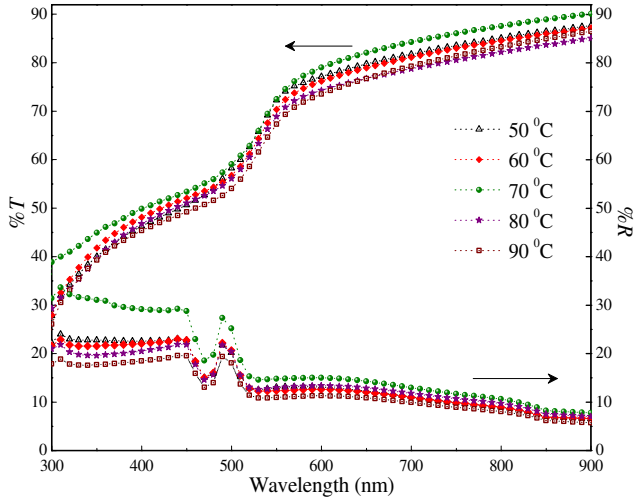

Figure 4. Optical $T\%$ and $R\%$ spectra of CdS nanofilms deposited at different T_d.

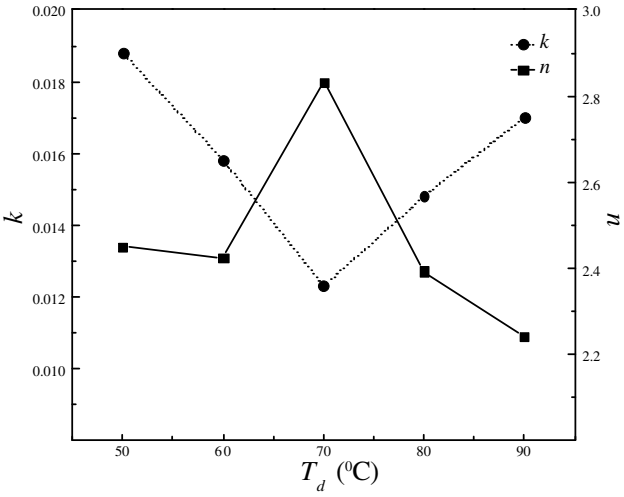

Figure 6. Variation of k and n of CdS nanofilms as a function of T_d.

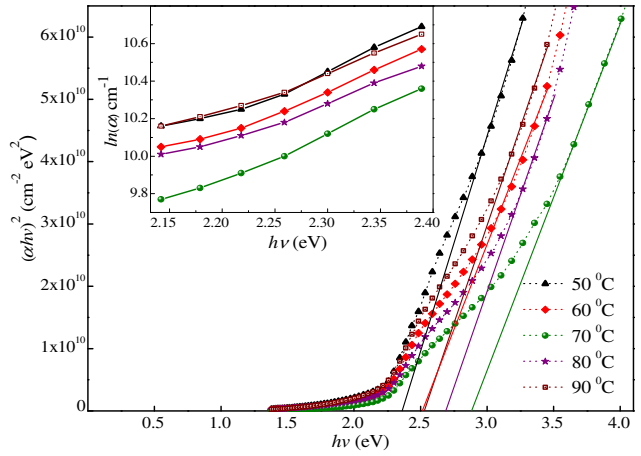

Figure 5. $(\alpha h\nu)^2$ versus $h\nu$. Inset shows a plot for E_u.

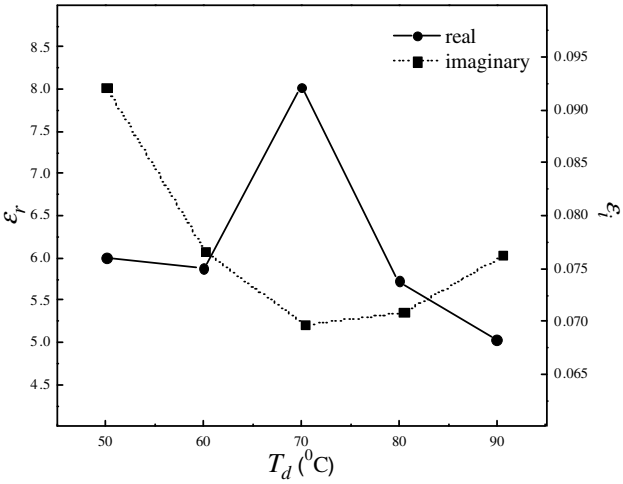

Figure 7. Dielectric constant (real and imaginary) of CdS nanofilms as a function of T_d.

we see a polymorph (cubic/hexagonal) CdS structure for $T_d = 70\,^\circ$C. For films deposited above 70 °C, an increase of the hexagonal phase is evident from the appearance of other reflections peaks associated with α-CdS phase in the polymorph. The d_{hkl} increase with a rise of T_d may be attributed to phase alteration from cubic to polymorph. The structure formation under the influence of T_d can be discussed in terms of deposition activation energy (E_a) using the Arrhenius equation [11] (figure 8). The values of E_a have been observed to be 0.147 eV for T_d ranging from 50 to 70 °C and 0.072 eV for $T_d = 70$ to 90 °C respectively. The high value of E_a promotes cluster by cluster growth leading to a cubic structure, whereas a low E_a value corresponds to ion by ion growth favoring hexagonal structure [11]. The chemical reactions are temperature dependent. For T_d(= 50–70 °C), E_a has positive value and this deposition temperature range accelerates the chemical reaction. A further increase in T_d (70–90 °C) leads to the negative E_a values, suggesting that the reaction process may be slowing down.

This negative E_a value for CdS growth for temperatures 70–90 °C suggest that there is no energy barrier to the growth, but rather that this may be due to some other factors such as running out of reactants, steric hindrance, increased desorption, etc.

The film thickness (t) increases with increasing T_d from 50 to 70 °C to saturation, followed by a decrease (inset of figure 8). EDAX spectra (figure 9) and analysis indicates that the films deposited at $T_d < 70\,^\circ$C are rich in sulfur content while films deposited at $T_d > 70\,^\circ$C are rich in cadmium.

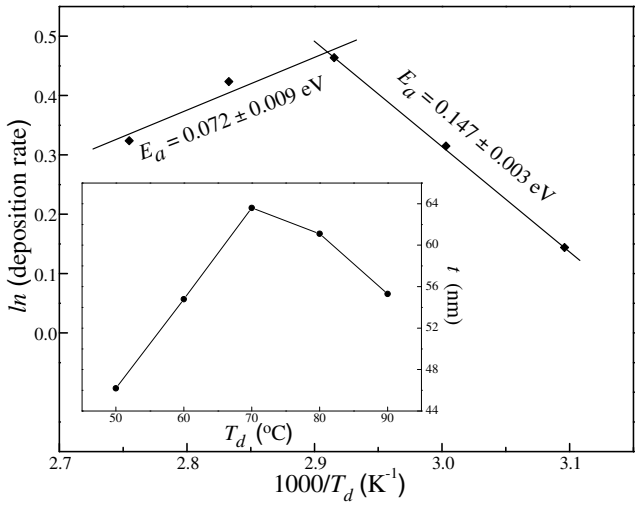

Figure 8. Arrhenius plot of the deposition rate as a function of the inverse of T_d. Inset shows the variation of t with T_d.

The ratio Cd/S (at.%)→ 1.0 as $T_d \rightarrow 70\,^{\circ}$C (figure 9) and the film becomes homogeneous in nature. The change in the composition of nanofilms may be associated with the availability of free Cd^{2+} and S^{2-} ions in the reaction solution at different T_d. The variation in deposition temperature significantly influences the structural properties of the CdS nanofilms. As T_d increases from 50 to 70 °C, D_v decreases while ε_{hkl} and δ_{hkl} increases (table 1). For $T_d = 70\,^{\circ}$C, D_v decreases to minimum while ε_{hkl} and δ_{hkl} increase to maximum. For $T_d > 70\,^{\circ}$C, D_v increases while ε_{hkl} and δ_{hkl} decrease. The high dislocation density and microstrain at $T_d = 70\,^{\circ}$C may be attributed to the restriction in dislocations and their movement within grain dimensions [33].

In figure 2, the nanocrystallites are uniformly distributed in the background throughout the surface which produces a densely packed film structure. Nanocrystallites having spherical symmetry are closely packed to each other indicating good adhesiveness with the substrate. There is presence of few clusters, due to agglomeration of crystallites which remain attached to the surface even after deposition cleaning.

AFM images of films deposited for $T_d < 70\,^{\circ}$C in figure 3 have spherical clusters packed together. The spherical crystallites have a regular size distribution at $T_d = 70\,^{\circ}$C and acquire a definite hexagonal shape for $T_d \rightarrow 90\,^{\circ}$C. The crystallite size and surface roughness decrease for $T_d = 50$–$70\,^{\circ}$C followed by an increase for $T_d > 70\,^{\circ}$C. The surface feature for $T_d = 90\,^{\circ}$C (figures 3(e) and (f)) shows the vertical growth of crystallites which acquire columnar structure, indicating a wurtzite-CdS structure. The deposition proceeds through nucleation, subsequent coalescence and vertical growth.

At a low deposition temperature ($T_d = 50\,^{\circ}$C), ionic species are less thermally activated with slow nucleation. However, the concentration of nucleation sites is large which may be attributed to a high value of E_a. As a result, coalescence of nuclei is more prominent which gives rise to large crystallite configuration in a cluster form. The SEM micrograph, figure 2(a), shows compact aggregates of crystallites with non-uniform size distribution. These clusters make large size crystallites with high surface roughness (see AFM image figure 3(a)). The SEM micrograph (figure 2(b)) for film deposited at $T_d = 60\,^{\circ}$C shows a reduction in crystallite size and uniformity in cluster distribution leading to low surface roughness as in the AFM image (figure 3(b)). Further at $T_d = 70\,^{\circ}$C, the coalescence period decreases due to a fast release of ions from the solution due to thermal activity. There is a limited nuclei size enlargement blocked by surrounding nuclei. Therefore, ion by ion growth becomes prevalent with a higher deposition rate. This leads to homogeneous nanocrystallites and low surface roughness for the film at $T_d = 70\,^{\circ}$C. The SEM micrograph (figures 2(c) and (f)) shows uniform distribution of crystallites separated by well defined grain boundaries with only a few clusters on the film surface supported by the appearance of empty space between uniformly distributed crystallites in figure 3(c). This may be due to a vast surface energy of nanocrystallites. However, for $T_d > 70\,^{\circ}$C, the deposition rate becomes slower due to rapid precipitation on the fast movement of ions in the solution and the decrease of pH on ammonia evaporation. Thus, a small value of E_a results in a low concentration of nuclei sites, which enables these sites to grow non-homogeneously and attain a large size. The SEM image (figure 2(d)) for $T_d = 80\,^{\circ}$C indicates a reduction in grain boundaries due to the growth of crystallites with increasing T_d. These large size crystallites are distributed non-uniformly and result in a high root mean square surface roughness (see AFM image, figure 3(d) and table 1). For $T_d = 90\,^{\circ}$C, the SEM image (figure 2(e)) indicates non-uniform crystallite distribution with an increase in compactness and crystallite growth. The corresponding AFM image (figure 3(e)) clearly shows large size hexagonal crystallites with a high surface roughness (table 1).

All films under investigation exhibit high transmittance (>70%) and low reflectance (<20%) in the Vis–NIR region (figure 4). This makes these nanofilms a good candidate for different optoelectronic applications. In visible wavelength range (400–700 nm), for $T_d = 70\,^{\circ}$C the nanofilm shows maximum T% and R%. The value of α decreases to minimum for $T_d = 70\,^{\circ}$C (table 2). The high values of α may be attributed to large grain size, non-stoichiometric nature and enhanced light scattering due to large surface roughness (figures 2(c) and 3(c)). From figure 5, a sub-band gap (E_g^{sub}) exists along with a band gap which may be due to disorder and an amorphous component in the deposited nanofilms. This E_g^{sub} refers to the transition related to the band tails [24, 34]. The values of E_g^{sub} are given in table 2. The value of E_g (table 2) increases to maximum for $T_d = 70\,^{\circ}$C and can be explained in terms of band edge sharpness (B) and Urbach energy (E_u). The values of B (table 2) are evaluated from the plot of α^2 versus hv in the region of band to band absorption (not shown here) [32]. B decreases to minimum while E_g increases to maximum as T_d increases from 50 to 70 °C. This may be attributed to the reduction in crystallite size and an increase in the homogeneity of the film structure with an increase in deposition temperature. The increase in B and decrease in E_g for $T_d > 70\,^{\circ}$C may be attributed to phase alteration and the rise of inhomogeneity due to increasing crystallite size. Liu *et al* have reported a cubic to hexagonal transformation of CdS films and a continuous decrease in the optical band gap from 2.56–2.38 eV with increasing

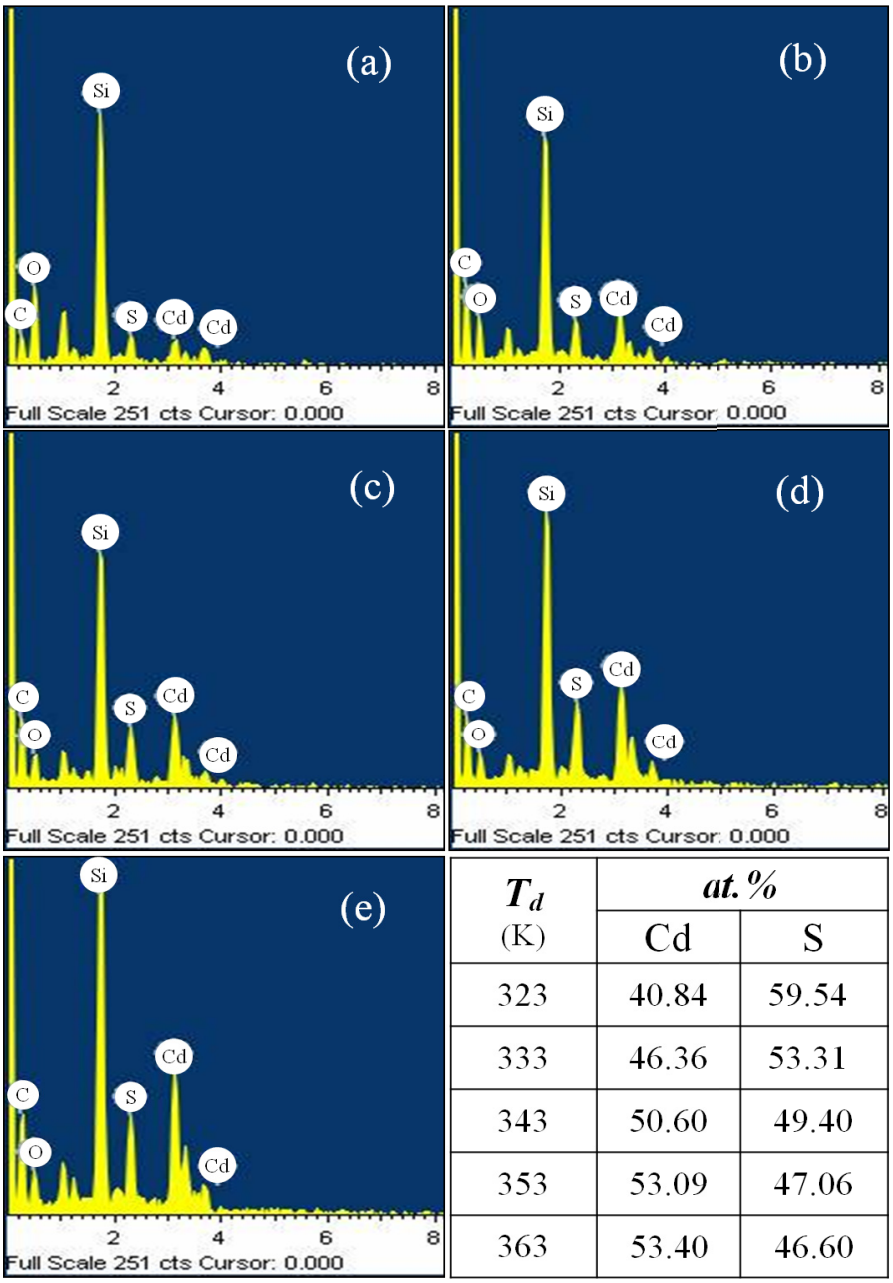

T_d (K)	at.%	
	Cd	S
323	40.84	59.54
333	46.36	53.31
343	50.60	49.40
353	53.09	47.06
363	53.40	46.60

Figure 9. EDAX spectra for CdS nanofilms deposited at (a) 50 °C, (b) 60 °C, (c) 70 °C, (d) 80 °C and (e) 90 °C with quantized value in at.%.

deposition temperature from 55–85 °C [24]. Wenyi *et al* have observed an improvement in the surface morphology and a decrease in the optical band gap (2.56–2.336 eV) of CdS films with an increase in deposition temperature (65–95 °C).

The variation observed in E_g with T_d may be due to a change in concentration of defects (e.g. vacancies, interstitials etc.) causing lattice deviation associated with phase alteration. These defects may act as trap centers for radiations and affect the absorption [3]. Low values of E_g for $T_d \neq 70$ °C may be associated with defect induced band tailing due to the creation of localized energy states near the band edges. The width of these band tail states can be described by E_u [32]. The values of E_u (table 2) calculated using the plot $\ln \alpha$ versus $h\nu$ decrease to minimum for $T_d = 70$ °C (inset of figure 5). The high values of E_u indicate structural disorder [35], creating more and more localized states within the band tails of the valance and conduction band due to a large grain dislocation density (table 1) and vast surface energy associated with the existence of nanocrystallites.

In the visible spectral region, the maximal value of n and minimal for k at $T_d = 70$ °C can be explained on the basis of the minimum value of α (table 2). The homogeneous and smooth surface of films deposited at $T_d = 70$ °C (figures 2(c) and 3(c)) explains the small k and high n values. For films deposited at $T_d \neq 70$ °C, large surface roughness and inhomogeneity in films results in high α values responsible for high k and small n values. Since, ε_r and ε_i depend upon n and k, therefore in the visible spectral region they vary similar to n and k with increasing T_d (figure 7). The imaginary component of a complex dielectric constant, which signifies dielectric loss, shows a minimum and a real component indicating dielectric efficiency attains a maximum at $T_d = 70$ °C. The values of ε_r and ε_i for CdS nanofilms, in the visible spectral region, have been found to vary from 5.026 to 8.020 and 0.070

to 0.092, respectively. The optical conductivity (σ) describes the response of the material to electromagnetic radiations. The optical conductivity is proportional to absorption energy and has been determined [32] (table 2). The optical conductivity is minimum for $T_d = 70\,^{\circ}\mathrm{C}$ associated with a polymorph structure of films exhibiting low α and high n due to good homogeneity and high stoichiometry (figure 9). The large values of σ for $T_d \neq 70\,^{\circ}\mathrm{C}$ may be attributed to high α due to the presence of defects, non-stoichiometry, surface roughness and the large size of crystallites in the films.

The use of CdS nanofilms under investigation as an optical filter for photovoltaic application necessitates the requirement of high transmittance and low absorbance with a higher band gap. These nanofilms (thickness= 45–65 nm) have the band gap range 2.43–2.88 eV with a high $T\%$ (>70%) and low $R\%$ (<20%) in the wavelength region 400–900 nm. The thickness of an optical filter strongly affects the performance of the photovoltaic device i.e. allowing almost free transmission of the solar spectrum.

5. Conclusion

In this work, the influence of T_d on structural, morphological and optical properties of CBD deposited CdS nanofilms has been investigated. XRD analysis indicates that nanofilms exhibit cubic and polymorph structures depending upon deposition temperature. SEM and AFM analysis shows that the nanofilms have dense and uniform surface morphology, free from pores and cracks. The values of E_g and n show a maximum for $T_d = 70\,^{\circ}\mathrm{C}$ with a corresponding minimum in disorder parameter (B), Urbach energy (E_u) and extinction coefficient (k). The high optical conductivity has been observed. For $T_d = 70\,^{\circ}\mathrm{C}$ the nanofilm exhibits low crystallite size (~20 nm), surface roughness and high stoichiometry. CdS nanofilms grown at 70 °C have high transmittance, low absorbance with a higher band gap and may be suitable for enhancing solar cell performance.

Acknowledgments

The authors acknowledge WIHG, Dehradun, IIT-Roorkee, HPU Shimla and JUIT Solan for providing SEM+EDAX, AFM, XRD and UV–Vis–NIR facility, respectively.

References

[1] Ennaoui A 2013 *Renew. Energy* **49** 68–71
[2] Ganeev R A, Ryasnyansky A I, Tugushev R I and Usmanov T 2003 *J. Opt. A: Pure Appl. Opt.* **5** 409–17
[3] Chandramohan S, Kanjilal A, Tripathi J K, Sarangi S N, Sathyamoorthy R and Som T 2009 *J. Appl. Phys.* **105** 123507
[4] Hur S G, Kim E T, Lee J H, Kim G H and Yoon S G 2008 *J. Vac. Sci. Technol.* B **26** 1334–7
[5] Kumar S, Kumar S, Sharma P, Sharma V and Katyal S C 2012 *J. Appl. Phys.* **112** 123512
[6] Wei T Y, Huang C T, Hansen B J, Lin Y F, Chen L J, Lu S Y and Wang Z L 2010 *Appl. Phys. Lett.* **96** 013508
[7] Qin H, Zhao Y, Liu H, Gao Z, Wang J, Liu D, Sang Y, Yao B and Boughton R I 2011 *J. Solid State Chem.* **184** 725–8
[8] Perez R M, Hernandez J S, Puente G C and Galan O V 2009 *Sol. Energy Mater. Sol. Cells* **93** 79–84
[9] Pradhan B, Sharma A K and Ray A K 2009 *J. Phys. D: Appl. Phys.* **42** 165308
[10] Minemoto T, Takakura H and Hamakawa Y 2006 *Sol. Energy Mater. Sol. Cells* **90** 3576–82
[11] Moualkia H, Hariech S, Aida M S, Attaf N and Laifa E L 2009 *J. Phys. D: Appl. Phys.* **42** 135404
[12] Chirila A *et al* 2011 *Nature Mater.* **10** 857–61
[13] Joshi R A, Ghosh A, Taur V S, Shaikh S U, Siddiqui F Y, Birajadar R B, Ghule A V and Sharma R 2011 *Mater. Chem. Phys.* **127** 191–6
[14] Saikia D, Saikia P K, Gogoi P K, Das M R, Sengupta P and Shelke M V 2011 *Mater. Chem. Phys.* **131** 223–9
[15] Romeo A, Terheggen M, Abou-Ras D, Batzner D L, Haug F J, Kalin M, Rudmann D and Tiwari A N 2004 *Prog. Photovolt., Res. Appl.* **12** 93–111
[16] Mann J R, Vora N and Repins I L 2010 *Sol. Energy Mater. Sol. Cells* **94** 333–7
[17] Lazos C D G *et al* 2008 *J. Electrochem. Soc.* **155** D158–62
[18] Kumar S, Sharma P and Sharma V 2012 *J. Appl. Phys.* **111** 113510
[19] Barote M A, Yadav A A and Masumdar E U 2011 *Physica* B **406** 1865–71
[20] Roy P and Srivastava S K 2006 *Mater. Chem. Phys.* **95** 235–41
[21] Kariper A, Guneri E, Gode F, Gumus C and Ozpozan T 2011 *Mater. Chem. Phys.* **129** 183–8
[22] Begum A, Hussain A and Rahman A 2012 *Beilstein. J. Nanotechnol.* **3** 438–43
[23] Lu W, Huang P, Li K, Yan P, Wang Y and Yan B 2013 *Int. J. Electrochem. Sci.* **8** 2354–64
[24] Liu F, Lai Y, Liu J, Wang B, Kuang S, Zhang Z, Li J and Liu Y 2010 *J. Alloys Compounds* **493** 305–8
[25] Wenyi L, Xun C, Qiulong C and Zhibin Z 2005 *Mater. Lett.* **59** 1–5
[26] Mahmood A, Ahemed N, Raza Q, Khan T M, Mehmood M, Hassan M and Mahmood N 2010 *Phys. Scr.* **82** 065801
[27] Cullity B D 1978 *Elements of X-Ray Diffraction* (New York: Addison-Wesley)
[28] Williamson G K and Smallman R E 1956 *Phil. Mag.* **1** 34–45
[29] Kumar S, Sharma P and Sharma V 2012 *J. Appl. Phys.* **111** 043519
[30] Perkins C L and Hasoon F S 2006 *J. Vac. Sci. Technol.* A **24** 497–504
[31] Borse S V, Chavhan S D and Sharma R 2007 *J. Alloys Compounds* **436** 407–14
[32] Sharma P and Katyal S C 2007 *J. Phys. D: Appl. Phys.* **40** 2115–20
[33] Choi Y and Suresh S 2002 *Acta Materia.* **50** 1881–93
[34] Akyuz I, Kose S, Atay F and Bilgin V 2006 *Semicond. Sci. Technol.* **21** 1620–6
[35] Vigil O, Riech I, Rocha M G and Angel O Z 1997 *J. Vac. Sci. Technol.* A **15** 2283–6